A Multilevel-DC-Link Converter With Single-Device Modules in Series for VSC-HVDC Application

Ruihang Bai, *Graduate Student Member, IEEE*, Biao Zhao, *Senior Member, IEEE*, Xueyin Zhang, Lu Qu, *Member, IEEE*, Jinpeng Wu, Zhanqing Yu, *Member, IEEE*, Qiang Song, *Senior Member, IEEE*, and Rong Zeng, *Senior Member, IEEE*

***Abstract*—Voltage-source-converter-based high-voltage dc transmission (VSC-HVdc) is widely applied in the fields such as offshore wind power transmission, and modular multilevel converter (MMC) is a common converter for it. The large capacitors and numerous devices in MMC limit its technical economics. In comparison, the multilevel dc-link converter with single-device-modules in series (abbreviated as MDC) proposed in this article may have advantages in terms of volume, as well as the potential in cost and efficiency. The single-device modules (SDM) solve the problems on both voltage sharing and floating supply. The current model of MDC is analyzed, and the commutating process in MDC is discussed in detail. The SDMs perfectly match with the characteristics of the quasi-soft switch in MDC, maintaining energy balance during operation without overvoltage or undervoltage. Finally, a high-power MDC prototype of 6.2 MVA is innovatively implemented and comprehensively tested to verify the theoretical commutation analysis and feasibility of the proposal. The research is helpful for promoting the application of MDC in VSC-HVdc, thus further improve the competitiveness of VSC-HVdc.**

***Index Terms*—AC/DC conversion, multilevel dc-link converters (MDCs), series connection, voltage-source-converter-based high-voltage dc transmission (VSC-HVdc).**

I. Introduction

OFFSHORE wind power is a renewable energy with wide source, which is getting more attention and has a rapidly growing installed capacity [1], [2], [3]. Voltage-source-converter-based high-voltage dc transmission (VSC-HVdc) plays a dominant role in its transmission due to the characteristics of flexible adjustment, applicability to submarine cables, and ability to provide synchronous voltage to connect wind turbines [4], [5], [6]. The modular multilevel converter (MMC) has been widely used in VSC-HVdc [7], [8], in which multilevel modulation is adopted to achieve great power quality, while significantly reducing the switching frequency to optimize efficiency. Besides, it avoids the technical bottleneck of series connection of power-electronic devices with hard switching behaviors.

The construction of series-connected submodules in MMC can be traced back to the cascaded STATCOM [9], in which the cascaded full-bridge modules are switched IN and OUT to generate multilevel ac waveforms. However, such topology cannot realize both public HV-dc and -ac buses concurrently, so it is not suitable for ac/dc conversion in VSC-HVdc. To solve this problem, MMC adopts six bridge arms to connect the three-phase ac terminals, compensating their voltage difference to construct a public dc bus. Since high energy pulsation of power-frequency exists in the bridge arms, huge capacitors in the submodules are necessary to balance it. In fact, the capacitors can account for over 50% and 80% of the total volume and weight of the submodules, respectively [10]. Therefore, the scale of converter platforms will be greatly increased, which is especially sensitive in offshore applications. In addition, the large quantity of power-electronic devices in MMC also leads to high costs. These factors reduce the technical economic of VSC-HVdc in offshore wind power application.

Flying-capacitors-based and cascaded-submodules-based multilevel dc-link inverter is originally discussed in [11]. Unipolar multilevel waveform of rectified sinusoid is modulated by the dc-link chain, and is further half-flipped by an H-bridge to generate an ac sinewave. Meanwhile, the inherent dc bias of the rectified sinusoid can naturally construct a public dc output, as is widely applied in dc/dc transformers [12], [13]. However, high voltage ripple of fundamental frequency exists in the dc port of the multilevel dc-link inverter, for which extremely large filter inductor is required, and thus, limits its application. A three-phase multilevel dc-link converter for VSC-HVdc application solves this problem by the series connection of the three-phases dc-link chains, as is proposed in [14]. Compared with MMC, in which two arms consist of half-bridge submodules in series to withstand double the peak ac voltage, respectively, is adopted in each phase, this scheme only needs one arm to withstand the peak voltage and an extra H-bridge to flip the voltage. Therefore, it has optimized device number, power loss, and especially, the minimized capacitance demand.

Manuscript received 15 August 2023; revised 19 October 2023 and 28 November 2023; accepted 15 December 2023. Date of publication 20 December 2023; date of current version 26 January 2024. This work was supported by the National Key R&D Program of China under Grant 2022YFB4200800. Recommended for publication by Associate Editor E. Babaei. *(Corresponding authors: Biao Zhao; Rong Zeng.)*

Ruihang Bai, Biao Zhao, Lu Qu, Jinpeng Wu, Zhanqing Yu, Qiang Song, and Rong Zeng are with the Department of Electrical Engineering, Tsinghua University, Beijing 100084, China (e-mail: brh20@mails.tsinghua.edu.cn; zhao-biao@tsinghua.edu.cn; qulu@tsinghua.edu.cn; jinpengwu@tsinghua.edu.cn; yzq@tsinghua.edu.cn; songqiang@tsinghua.edu.cn; zengrong@tsinghua.edu.cn).

Xueyin Zhang is with the Tsinghua Sichuan Energy Internet Research Institute, Chengdu 610200, China (e-mail: zhangxueyin@tsinghua-eiri.org).

Color versions of one or more figures in this article are available at https://doi.org/10.1109/TPEL.2023.3345019.

Digital Object Identifier 10.1109/TPEL.2023.3345019

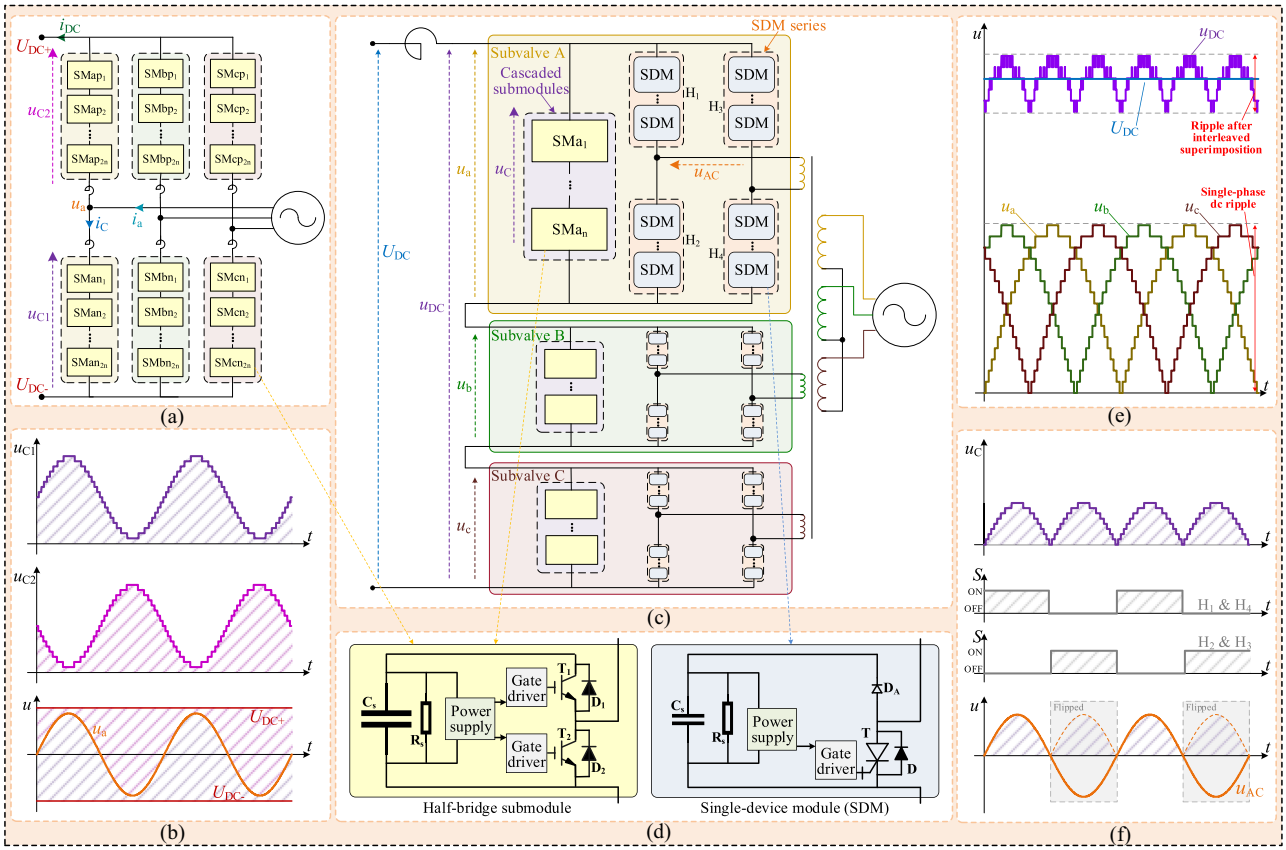

Fig. 1. Topology construction and operation principle of MDC. (a) MMC. (b) Alternating voltage generation in MMC. (c) Multilevel DC-link converter. (d) Proposed single-device modules. (e) Interleaved superimposition of voltage at DC-side. (f) Principle of AC/DC conversion in MDC.

A remaining bottleneck of this scheme in higher voltage application is the large number of fully controlled devices connecting in series in the H-bridge for voltage flipping. Although the H-bridge devices operate in zero-voltage switching (ZVS), the switched current is nonzero in some conditions, resulting in the voltage-sharing problem. In addition, a floating supply is required for the device drivers. Currently, such researches mainly focus on dynamic adjustment of gate signals [15], [16], active clamping [16], [17], chopper energy-consuming circuits [18], or active voltage-sorting control [19], which are too complex for HVdc applications with large device number, have limitations for integrated gate-commutated thyristor (IGCT) applications that may optimize the efficiency, and have not been designed coupling with the commutation characteristics of the topology.

Considering the situation above, this article proposes a multilevel dc-link converter with single-device-modules in series (abbreviated as MDC) for VSC-HVdc application, giving comprehensive research from the perspective of both operation principle and high-power hardware implementation. The rest of this article is organized as follows. In Section II, the topological evolution process of MMC to MDC is revealed, and a single-device module (SDM) suitable for series connection in H-bridges of MDC is proposed. In Section III, the current models on both kinds of bridge arms in MDC and the electrical stress of their devices in various modes are analyzed. Then in Section IV, the commutation processes of MDC with SDMs are discussed. Section V designs and implements a 6.2-MVA MDC power prototype, which is further comprehensively tested in Section VI. In Section VII, the performance of the proposal is discussed in detail. Finally, Section VIII concludes this article.

II. MDC With Single-Device Modules

A. Topology Construction of MDC

The topology of MMC is shown in Fig. 1(a). The bridge arms are connected between one dc port and one ac terminal. The upper and lower bridge arms generate dc-biased power-frequency sinusoidal voltage with the phase shift of 180° mutually to construct an alternating voltage in the common ac point, as in Fig. 1(b).

In comparison, the MDC is shown in Fig. 1(c). Three subvalves form a three-phase converter. In each subvalve, the rectified sinusoid is generated by the cascaded half-bridge submodules and then half flipped by the H-bridge to achieve ac output, as in Fig. 1(f). The dc ports of the subvalves are directly connected in series, while their ac ports are, respectively, connected to the three windings of the transformer.

Since the cascaded-submodules of the three subvalves can be decoupled controlled, they can operate with the phase shift of 120° to achieve three-phase output. Meanwhile, the dc voltage of three subvalves is interleaved superimposed, which not only substantially reduces the dc voltage ripple but also triples its

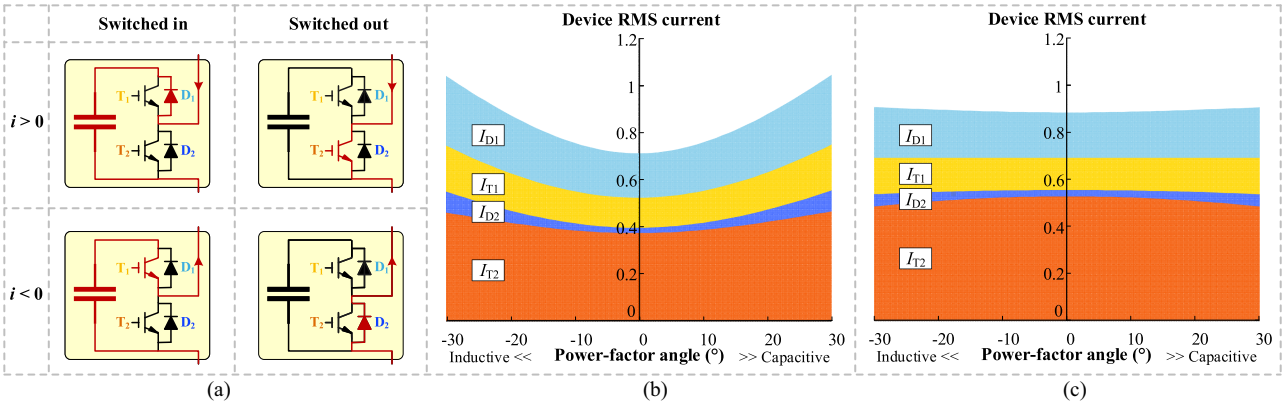

Fig. 2. Current model and distribution of cascaded-submodules in MDC. (a) Flowing device in half-bridge submodules under different current directions and switching modes. (b) Current distribution in cascaded-submodules of MDC (inverter mode). (c) Current distribution in submodules of MMC (inverter mode).

frequency, thus significantly lower the demand of the filter inductance, as in Fig. 1(e).

B. Proposed Single-Device Modules

In HVdc application, the series connection of devices in H-bridge is the technical bottleneck of MDC. An SDM for H-bridge is proposed, as shown in Fig. 1(d). It imitates the design of half-bridge submodules. Capacitors are applied not only to maintain voltage balance between devices but also realize the floating supply for secondary controller circuit in place of high-isolated multioutput transformers. In each SDM, the upper transistor is removed and the upper diode is replaced by a smaller one to charge the capacitor and replenish the costumed energy.

C. Characterization of Single-Device Modules

When the transistor in one SDM turns ON, the auxiliary diode cuts off to block the capacitor from discharging. Therefore, the capacitance can be much higher than that of the traditional *RC* and RCD absorption circuits without worrying about the power loss [20], [21]. It ensures good voltage sharing effect and reliable floating supply.

On the other hand, since the capacitor in SDM does not participate in balancing the energy pulsation of the bridge arm, its capacitance is much lower than the millifarad-level capacitors in the half-bridge submodules. Therefore, this capacitor does not significantly increase the total size and cost of the MDC, which will maintain a considerable advantage of MDC over MMC.

III. Current Model and Switching Operation in MDC

A. Evenly Distributed Current in Cascaded Submodules

In MDC, the cascaded submodules flow the difference current between ac side and dc side. The instantaneous current direction and switching state of each submodule further determines the specific device through which the current flows, as shown in Fig. 2(a).

Taking the inverter mode as an example, the root mean square (rms) current of the cascaded-submodule devices under different power-factor angles is obtained through weighting the current distribution between the upper and lower devices of each submodule by the instantaneous value of the unitized modulation wave (which determines the proportion of the switched-IN submodules) and considering the influence of the current direction (please see the Appendix for the detailed calculation method), as shown in Fig. 2(b). The current values are normalized with respect to the dc current under unit-power-factor operation. The results are compared with that of the MMC with the same capacity and dc voltage in Fig. 2(c). The total rms current of devices in MDC is significantly smaller than that in MMC under high power factor. In particular, the current is more evenly distributed among the devices MDC, thus helping to reduce the power loss and the specifications of the devices used.

Like MMC, the devices of cascaded submodules are always in the hard-switching mode with the operating voltage of the supporting capacitors. The switching frequency caused by modulation is twice the power frequency, providing higher degree of freedom for intermodular voltage equalization.

B. Quasi-Soft Switching in H-Bridge

The current distribution in H-bridge is strongly related to the operation mode, as in Fig. 3. In the pure-active-power rectifier mode, the current flows completely through the diodes, which is equivalent to a full-bridge diode rectifier. In inverter mode, the current flows completely through the transistors. Since the ac voltage and current have overlapped zero-crossing, exactly at which the upper and lower H-bridge arms switch, the switching behaviors of the devices are perfectly soft, as in Fig. 3(a) and (c). Such feature also brings benefits to the evolution of MDC in unidirectional conversion such as offshore wind-power, in which the transistors and diodes of different specifications can be applied in the H-bridge to further optimize the cost.

When the MDC also compensates reactive power to the grid, the ac current is phase-shifted. Therefore, the devices still switch at zero voltage, but the operating current is no longer zero. If the inductive var is output, regardless of the active-power direction, the transistors always turn OFF with nonzero current at zero voltage while the diodes commutate naturally, as in Fig. 3(b). When capacitive var is output, the contrary happens

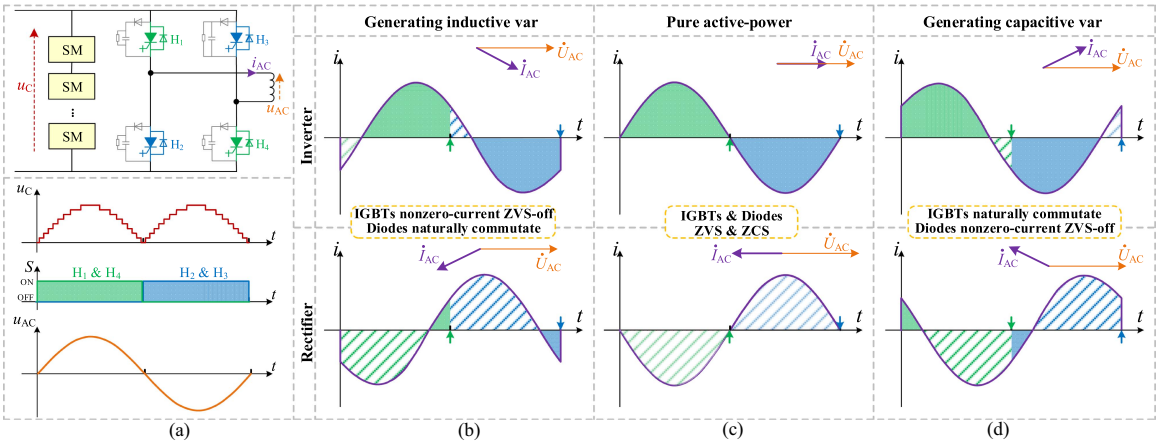

Fig. 3. Current model and switching behaviors of H-bridge in MDC. (a) Voltage waveform and reference direction of electrical quantity. Each H_n is equivalent to that in Fig. 1(c). (b) Inductive-var-generation mode. (c) Pure-active-power mode. (d) Capacitive-var-generation mode. In (b)–(d), filled color and shadow refer to current flowing through transistors and diodes separately.

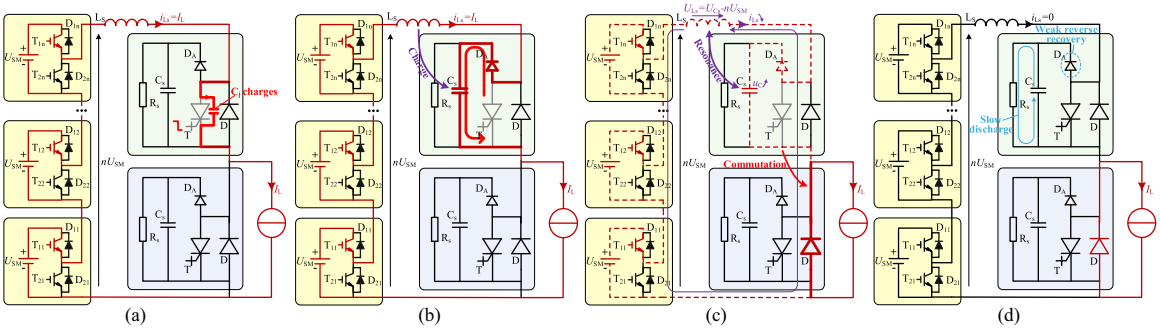

Fig. 4. Commutation process of hard turn-OFF behavior. (a) IGCT in H-bridge turns OFF. (b) Support capacitor in SDM charges. (c) Support capacitor resonances with stray inductor and current commutates to the opposite FWD. (d) Commutation ends.

[see Fig. 3(d)]. This commutation behavior is different from the common "zero current but nonzero voltage" soft turning-OFF, and its electrical stress is between that of the soft turning-OFF and the hard turning-OFF, which will be further analyzed in Section IV.

IV. Commutation Analysis of MDC

A. Hard Turn-Off Behavior

Considering a potential benefit on power loss, IGCT is adopted as the active device in the following analysis. To simplify the analysis, the commutation in only one pair of the arms in the H-bridge is considered, which is completely symmetric to that in the other pair.

The situation that IGCTs turn OFF with the cascaded-submodules modulating a nonzero voltage happens [see Fig. 4(a)] when fault causes MDC to emergency block. It is a hard turn-OFF commutation just like that in the MMC modules and pulsewidth modulation voltage-source converters (PWM-VSCs).

First, the equivalent junction capacitance of IGCT is quickly charged to the voltage of its support capacitor. Then the current of the stray inductor transfers to the positively biased auxiliary diode and charges the support capacitor, as in Fig. 4(b). The parasitic inductance of the capacitor and the forward recovery of the auxiliary diode result in an overvoltage on IGCT.

Thereafter, the voltage difference between the support capacitor and the bus bar caused by charging is imposed on the stray inductor, causing its current to drop continuously, which is equivalent to a resonance between the support capacitor and the stray inductor. The load current is enforced to transfer to the free-wheeling diode (FWD) of the opposite bridge arm [see Fig. 4(c)]. Finally, when the current of the stray inductor drops to zero, the auxiliary diode cuts off, meaning the end of the commutation. The weak reverse recovery of the auxiliary diode causes an insignificant pit in the waveform. The energy charged to the support capacitor will further be slowly dissipated by the floating supply and the static voltage-sharing resistance, as in Fig. 4(d).

B. Quasi-Soft Turn-Off Behavior

When MDC compensates inductive var to the grid, the IGCTs in each bridge arm operates with nonzero-current ZVS-off behavior at power frequency, as analyzed in Fig. 3(b). According to the principle of MDC, before the H-bridge switches, the cascaded-submodules have already modulated zero level, for which all the half-bridge submodules are switched OUT and the

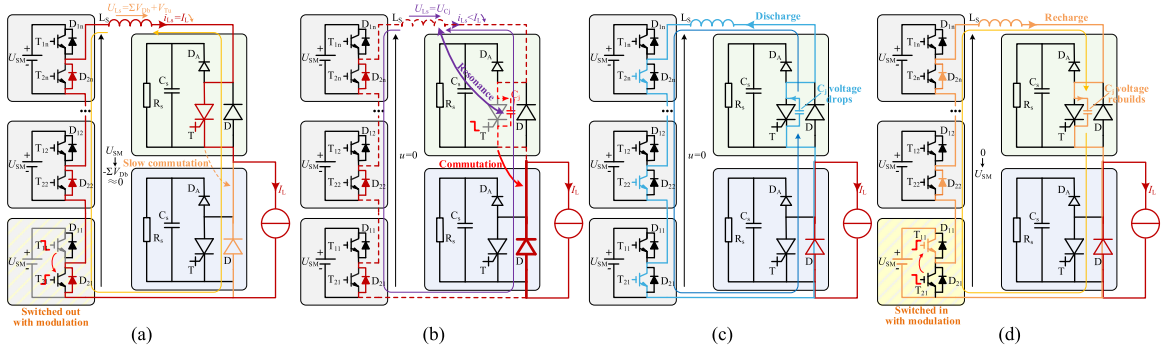

Fig. 5. Commutation process of nonzero-current ZVS-OFF behavior. (a) Cascaded-submodules modulate zero level. (b) IGCT in H-bridge turns OFF. Junction capacitor resonances with stray inductor and current commutates to the opposite FWD. (c) Junction capacitor of IGCT discharges and its voltage falls. (d) Cascaded-submodules switch IN and voltage of IGCT in H-bridge rebuilds.

lower pair of devices in them flows. Therefore, the load current distributes between the existing flowing circuit and the opposite FWD in H-bridge with the slow commutation rate decided by the sum of the voltage drop on the devices of the existing flowing circuit, as in Fig. 5(a).

Then when the IGCTs in the H-bridge turns OFF, the stray inductor first charges their junction capacitors. Due to the bus voltage of zero, the voltage on the junction capacitor is directly applied onto the stray inductance, causing its current to transfer to the opposite FWD [see Fig. 5(b)]. If the commutation process is not finished when junction capacitor charges to the voltage of that of the support capacitor, the auxiliary diode is briefly ON and the support capacitor is slightly charged.

With the end of the commutation, the junction capacitor of the turned-OFF IGCT discharges through the cascaded submodules and the opposite FWD, for which its voltage drops to zero again, as in Fig. 5(c). Finally, the voltage of that IGCT rebuilds along with the step modulation of the cascaded submodules [see Fig. 5(d)]. If each H-bridge arm is composed of multiple SDM in series, then the voltage distribution among them will be decided by the blocking resistance of the IGCTs since the static voltage-sharing resistors are in parallel with the support capacitors, respectively, rather than the IGCTs. Therefore, there may be temporarily imbalanced voltage due to the dispersion, which will nevertheless not be higher than the support capacitor voltage benefit from to the clamp of the auxiliary diode. When the cascaded-submodules get fully modulated at the peak of ac voltage, the supporting capacitor will be clamped and charged into the rated voltage.

It is noted that the voltage on IGCT rises due to the charging of junction capacitor, which overlaps a little with its current and leads to certain switching loss. Therefore, the turn-OFF energy is significantly lower than the hard turn-OFF condition (in which the current will not fall until the voltage rises higher than the bus voltage and leads to high switching loss), but is not strictly zero.

C. Quasi-Soft Recovery of Diodes

According to Fig. 3(d), diodes in H-bridge undergoes nonzero-current reverse recovery when MDC generates capacitive var. This process is more complicated.

As the last half-bridge submodule is switched OUT, the bus voltage turns zero, but the current does not change since the H-bridge has not switched [see Fig. 6(a)]. When IGCT in the H-bridge turns ON, the new path consisting of the cascaded-submodules and the turned-ON IGCT shares current with the existed flowing path at the slow commutation rate decided by the voltage drop on the flowing diode, as in Fig. 6(b). Not until the modulated level of cascaded-submodules rises will the rapid commutation proceed [see Fig. 6(c)] with the rate of

$$\frac{\mathrm{d}i_{\mathrm{Ls}}}{\mathrm{d}t} = \frac{U_{\mathrm{SM}}}{L_{\mathrm{S}}}. \tag{1}$$

When the commutation ends, the diode reversely recovers [see Fig. 6(d)]. Because of the lower bus voltage and di/dt than normal hard-switch behavior, the reverse recovery is soft, which reflects in a lower peak reverse-recovery current (I_{rr}). Then the reverse-recovery current decays, for which the stray inductor charges the junction capacitor of this diode and raises its voltage. Finally, the voltage of the diode gradually rises to the rated value with the further modulation.

In quasi-soft turning-OFF process, the commutation happens once the IGCT turns OFF. In comparison, in the quasi-soft recovery, the commutation will not proceed when IGCT turns ON until the modulated level of cascaded-submodules rises. Therefore, it is strictly a near-zero-voltage recovery for the diode. Due to the low bus voltage during the recovery, the di/dt can be easily restricted by the stray inductance without the necessity of additional inductors in the loop like the usual cases of the IGCT-based converters to protect the FWD [22], [23]. In addition, the limited reverse-recovery charge and the low peak reverse-recovery current seldom affect the converter.

D. Particularity of the Proposal in MDC

Due to the micro-henry class stray inductance in MDC rather than a high arm inductance like MMC, the current-continuation effect in commutation is significantly weakened. When one SDM turns OFF, its support capacitor is only briefly charged, and then the overvoltage forces the current to transfer to the opposite arm. Therefore, the commutation feature is more similar to that in the two-level PWM-VSCs and the submodules in MMC rather than the commutation between MMC arms.

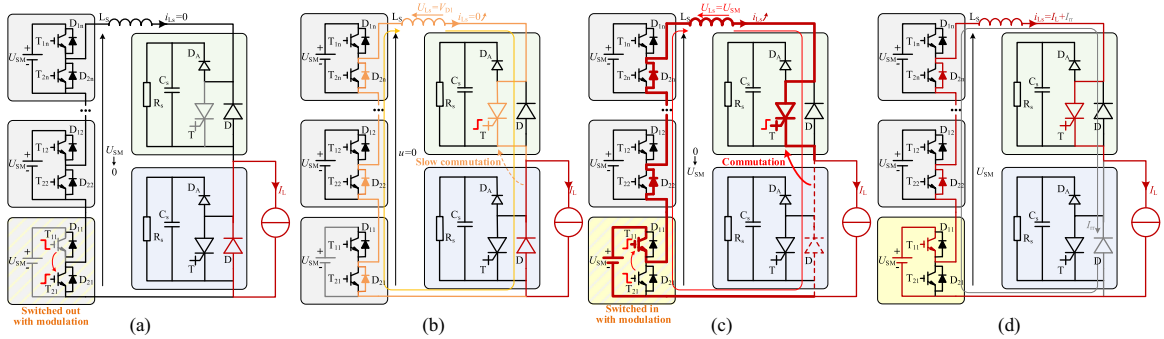

Fig. 6. Commutation process of near-zero-voltage recovery of diode. (a) Cascaded-submodules modulate zero level. (b) IGCT turns ON. Commutation with slow rate decided by voltage drop of flowing diodes. (c) Fast commutation as modulated level of cascaded-submodules rises. (d) Reverse recovery of diodes.

TABLE I
PARAMETERS OF THE DEVICES IN ONE SDM

Item	Parameter
IGCT	5SHY 42L6500
FWD	5SDF17L6500
Auxiliary diode	TMFDO 220-65
Support capacitor	30 μF*3 in parallel
Static voltage-sharing resistor	50 kΩ*2 in parallel
Floating supply	Custom-made (maximum 100-W output)

A comparison of Figs. 4(c) and 5(b) shows that the voltage on the turned-OFF IGCT is fully applied to the stray inductor for commutating in the ZVS mode due to the zero-voltage at the port of the cascaded-submodules. Besides, the junction capacitance is orders-of-magnitude lower than the support capacitor. Therefore, the commutation time of ZVS is short and the support capacitor hardly has charging effect. On the contrary, in the hard-switch process, the stray inductor inevitably charges the support capacitor. Luckily, this situation only solely exists in the blocking during fault. The energy in the support capacitor is continuously consumed by the floating supply and the static voltage-sharing resistor, which will be replenished when the cascaded-submodules are in full modulation. In conclusion, the proposal can continuously and stably operate in MDC, maintaining a balanced energy and letting the worrying about its overvoltage or undervoltage go.

V. IMPLEMENTATION OF HIGH-POWER MDC PROTOTYPE

An MDC prototype of single phase with the capacity of 6.2 MVA is innovatively implemented. The rated maximum bus voltage is 5400 V (realized by three 1800-V standard half-bridge modules in series) and the rated ac current is 1620 A. Each H-bridge arm consists of four SDMs, all of which are integrated in one valve to minimize the stray inductance and keep their consistency. The IGCTs is pressed back-to-back with its FWD, with water-cooled radiators in the middle. The SDMs are divided by FR-4 saucers to realize isolation, as shown in Fig. 7(a) and (b). Detailed parameters of devices in each SDM are shown in Table I.

Furthermore, the volume of MDC and MMC under the same capacity is compared in Fig. 8. One phase of MMC includes two arms, each of which withstands double the peak ac phase voltage.

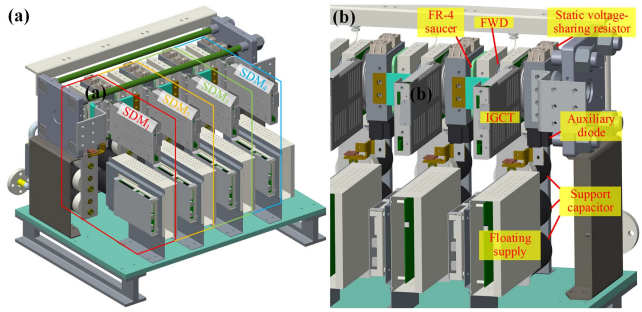

Fig. 7. Prototype design on H-bridge. (a) Four SDMs integrated in one valve. (b) Zoom-in graphic for details.

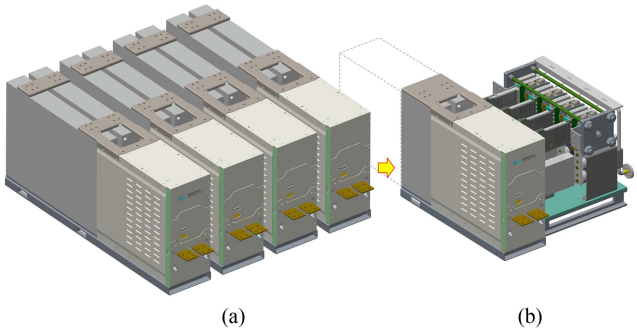

Fig. 8. Comparison between MMC and MDC on volume. (a) Four submodules of MMC. (b) One half-bridge submodule with reduced support capacitor and a four-SDMs-integrated H-bridge valve of MDC.

Therefore, four submodules in MMC are equivalent to one cascaded-submodule plus an H-bridge [with one SDM to form each arm, for which an H-bridge equals to one valve in Fig. 7(a)]. Since the support capacitance in cascaded-submodules is also lower than that of MMC submodule, the total volume of the MDC is significantly reduced.

VI. EXPERIMENTAL VERIFYING

A. Comprehensive Experimental Platform on MDC

An experimental platform is built to verify the theoretical analysis on commutation process, as well as the feasibility of

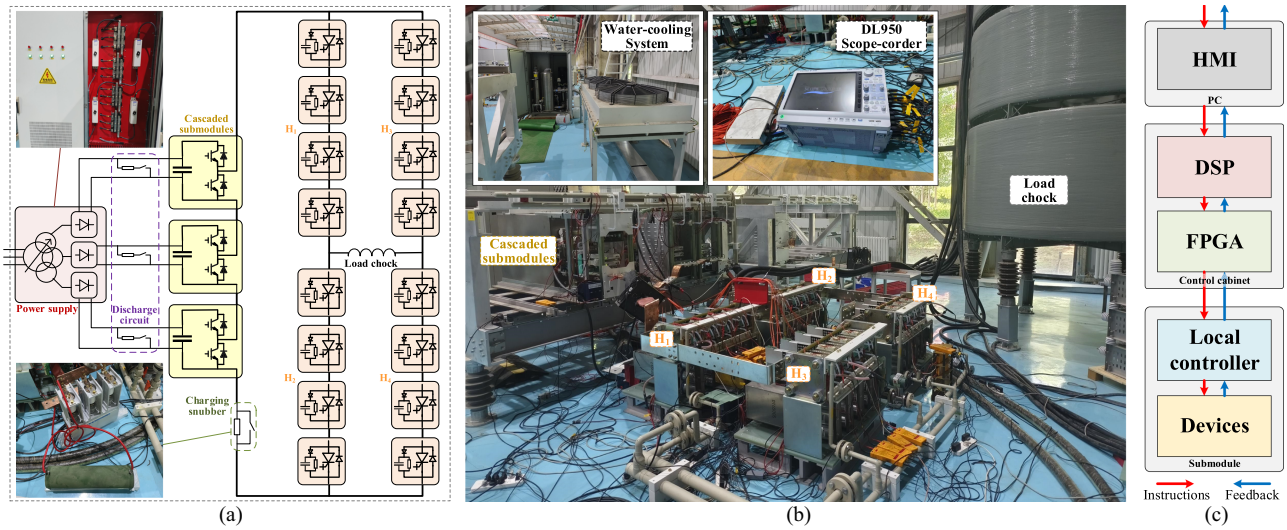

Fig. 9. Comprehensive experimental platform of MDC. (a) Experiment circuit. (b) Photograph of the whole platform. (c) Architecture of the controller.

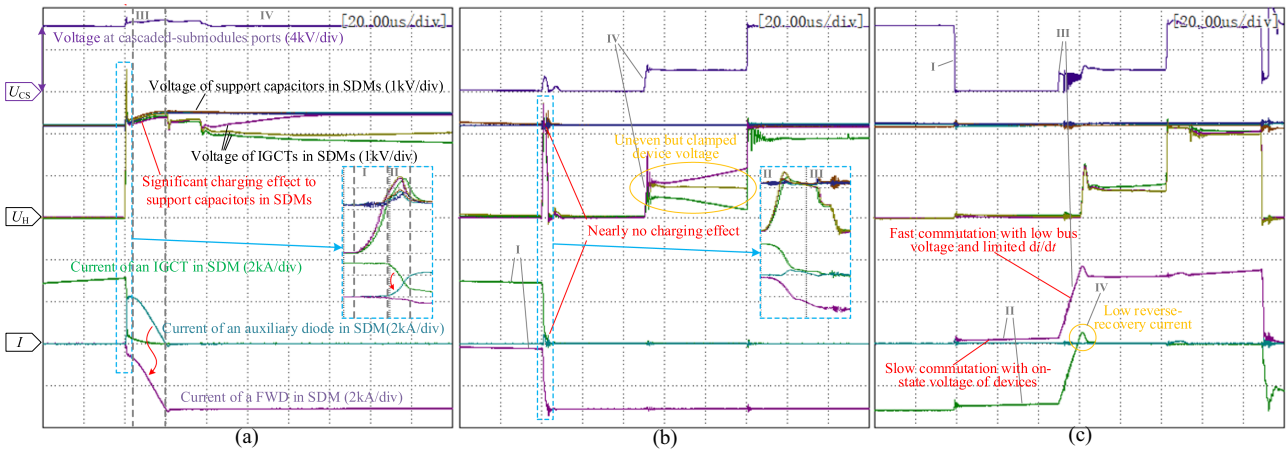

Fig. 10. Waveforms of double-pulse test. Subgraphs (a)–(c), respectively, correspond to the dynamic processes in Figs. 4–6, in each of which the numbers I-IV refers to the commutation behavior of subgraphs (a)–(d) in Figs. 4–6 separately. (a) Hard turn-OFF behavior. (b) Nonzero-current ZVS-OFF behavior. (c) Near-zero-voltage recovery of diode.

the proposed SDM and the implemented prototype. The circuit and photo of the whole platform are shown in Fig. 9(a) and (b) separately.

A transformer with three secondary windings supplies the system through respective rectifier bridges. A water-cycling machine helps to cooling the devices. High-insulation differential voltage probes and Rogowski coils detect the electrical quantities and send them to a DL-950 scope-recorder.

A four-level open-loop controller is developed for the experiment, which includes a human–machine interface (HMI) in PC, a control cabinet includes one DSP and one FPGA, and several local controllers in each of the submodules, as in Fig. 9(c). The instructions such as amplitude and phase angle are input to the HMI and sent to the DSP. Then the DSP generates the modulation waveform and transmit it to the FPGA, which connects to the local controllers and distributes the switching signals. Finally, the local controllers trigger the power-electronic devices. The operation states are also conveyed backward to realize a fault protection in the DSP.

B. Double-Pulse Test

A 1-mH chock is set at the ac port. The IGCTs in H_2 and H_3 arms keep in off-state, while those in H_4 arm keep in ON-state. All the cascaded-submodules are switched IN and two sequential pulses are sent to IGCTs in H_1 arm to test the hard turn-OFF behavior. Furthermore, the cascaded-submodules are switched OUT at the end of the first pulse or the gap between the two pulses to construct a zero bus-voltage for testing the quasi-soft turn-OFF and recovery behaviors.

The results are shown in Fig. 10(a)–(c), respectively, in which the key processes are marked corresponding to the theoretical analysis. The waveforms brilliantly accord with the process shown in Figs. 4–6.

TABLE II
POWER LOSS ANALYSIS ON H-BRIDGE

Maximum bus voltage (V)	AC current (A)	Inlet / outlet temperature (°C)	Measured power loss (kW)	Theoretical on-state loss (kW)
2400	720	36.2/36.6	1.176	2.495
3600	1080	36.4/37.5	3.234	4.132
4050	1250	37.4/38.9	4.410	4.995
4800	1400	39.7/41.6	5.586	5.804
5400	1620	40.4/42.8	7.056	7.073

In the hard turn-off behavior, the voltage of IGCTs rises as the IGCTs are turned OFF [Fig. 10(a)-I and Fig. 4(a)]. Once it is equal to the voltage of supporting capacitor, the current transfers to the auxiliary diode [Fig. 10(a)-II and Fig. 4(b)] and then commutates to the opposite diode [Fig. 10(a)-III and Fig. 4(c)]. During process, the supporting capacitors are charged significantly and its voltage rises obviously, which will be slowly dissipated by the resistor R_s [Fig. 10(a)-IV and Fig. 4(d)].

In the nonzero-current ZVS-off behavior, the current of IGCTs slowly commutates to the opposite diodes as the cascaded-submodules modulate zero level [Fig. 10(b)-I and Fig. 5(a)]. Once the IGCTs turn OFF, the fast commutation happens and the junction capacitor of IGCT is charged [Fig. 10(b)-II and Fig. 5(b)], which is then discharged when the commutation ends [Fig. 10(b)-III and Fig. 5(c)]. Finally, the voltage on IGCTs rebuilds as cascaded-submodules switch IN [Fig. 10(b)-IV and Fig. 5(d)].

In the near-zero-voltage recovery of diode, the cascaded-submodules modulate zero level [Fig. 10(c)-I and Fig. 6(a)] and the slow commutation begins [Fig. 10(c)-II and Fig. 6(b)]. Not until the cascaded-submodules switch IN will the fast commutation happen [Fig. 10(c)-III and Fig. 6(c)]. Finally, a weak reverse recovery of the diodes announces the end of the dynamic process [Fig. 10(c)-IV and Fig. 6(d)].

The test results verify the correctness of the theoretical analysis of the commutation.

C. Power-Cycling Experiment

The ac load is then replaced by a 7.5-mH chock. The prototype is operated with full inductive var generating and the power supply replenishes its power loss. Once the thermal stability is reached, the source voltage is raised repeatedly until the rated value.

Thermometers and flowmeters are set at the inlet and outlet of the cooling-water pipe in one H-bridge arm. With the constant flow velocity of 42 L/min, the loss of the bridge arm is calculated from the temperature rise between inlet and outlet. The results are compared with the calculated theoretical ON-state loss, as shown in Table II. The measured values are in good agreement with the theoretical ones at high load rate, and is lower at light load due to the use of device model with threshold voltage and slope resistance, in which the ON-state voltage drop is higher than the actual value at low current.

The waveforms under the full load of 5400-V maximum bus voltage and 1620-A ac current are shown in Fig. 11. It indicates

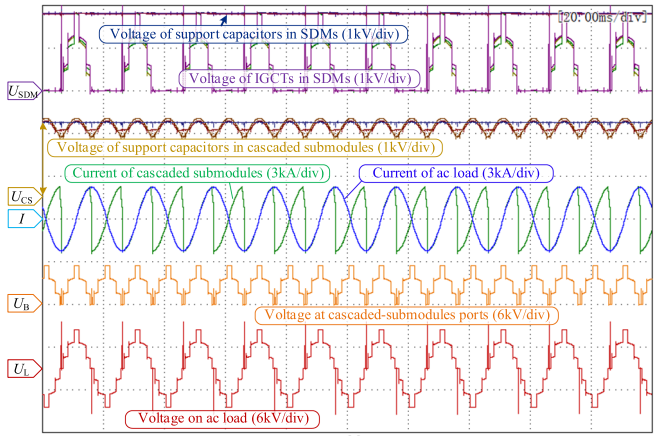

Fig. 11. Waveform of power-cycling experiment at full load (maximum bus voltage of 5400 V and AC current of 1620 A).

that the proposal achieves a good voltage sharing in the SDM-based H-bridge arms.

It is observed that spike exists in the voltage waveforms of the IGCTs and the ac lode. It is caused by the charging effect of the stray inductance to the junction capacitor in the nonzero-current ZVS-off behavior, as is analyzed in Fig. 5. Since the spike is clamped by the supporting capacitor and the auxiliary diode in each SDM, its peak value is below the rated voltage of the SDM, for which the devices will not breakdown. Furthermore, the total spike will not be higher than the peak ac voltage, so the ac-side equipment is safe. Despite this, the du/dt of this spike may break the insulation of the transformer, which needs to be designed carefully.

In the further continuous operation of 90 min, the equipment remains stable and reliable.

VII. DISCUSSION ON PERFORMANCE

A. Quantity of Components

Denoting the rated dc voltage as U_{DC}, in MDC, the voltage withstood by each bridge arm follows:

$$U_{\mathrm{arm}} = \frac{U_{\mathrm{DC}}/3}{2/\pi}. \tag{2}$$

Considering the redundancy rate of r, the number of series-connected submodules in each arm can be calculated by

$$n_{\mathrm{SM}} = \frac{U_{\mathrm{arm}}}{U_{\mathrm{SM}}} \times (1+r) \tag{3}$$

in which U_{SM} stands for the rated voltage of each submodule. Since one cascaded-submodule arm and four H-bridge arms are included in each subvalve of the three phases, the total device quantity is 18 times the n_{SM}.

The analysis of MDC and MMC as follows are based on a $\pm$500 kV, 2000-MVA system, in which the rated voltage regulation ratio is $\pm$10% and the maximum reactive-power output is 0.5 p.u. The IEGT ST2000GXH31 by Infineon [24] is applied in both the cascaded-submodules of the MDC and the MMC, and the reverse-conducting IGCT 5SHX-36L4521 by ABB [25] is

TABLE III
COMPONENT QUANTITY OF MDC AND MMC

Component	MDC	MMC
Fully controlled device	1500 IEGTs + 3000 IGCTs	5592
Total supporting capacitor	7.386F (Cascaded submodules) + 0.15F (H-bridge)	41.938F
Number of submodules*	3750	2796
Others	3000 of auxiliary diodes	-

*Equal to the number of floating supplies, local controllers, and static voltage-sharing resistors.

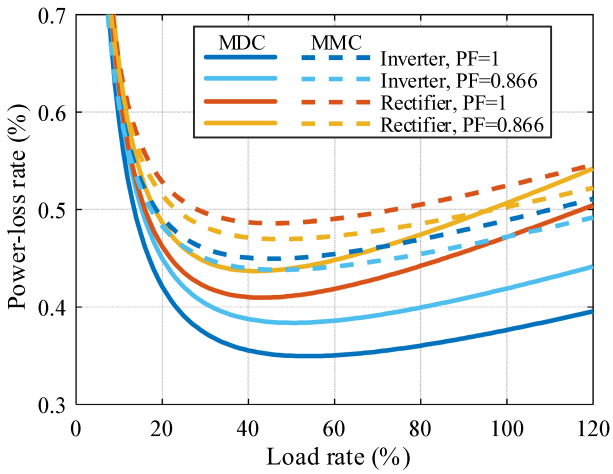

Fig. 12. Comparison of loss rate between MDC and MMC under various operation conditions. When power factor (PF) = 0.866, the converter compensates 0.5 p.u. inductive var to the AC grid.

applied in the H-bridge of the MDC. The rated voltage of all the submodules is set as 2200 V [26]. In each arm, a 5% redundancy of submodules is retained.

The energy pulsation in each arm can be calculated by integrating the product of its voltage and current, and then the capacitor demand can be obtained on the basis of ±5% voltage ripple. The results are shown in Table III.

The increase of submodule number rises the quantity of appending components, which leads to larger size and higher cost than the monolithic-device-based scheme. Despite this, the reduction of more than 80% supporting capacitor and nearly 20% fully controlled devices (and their gate-drivers) in MDC will still provide certain advantages over MMC.

B. Power Loss

The power loss of MDC is further calculated [27], [28], and is compared with that of MMC. The results under various operation modes and load rates are shown in Fig. 12. Since the cascaded submodules in MDC modulates in double the power frequency, its average switching frequency is set as 150 Hz and the frequency of MMC is set as 100 Hz, considering the dynamic voltage-sharing strategy [29].

At most of the load rates and operation modes, MDC shows a lower power loss than MMC. At full load rate, the loss rates of MDC under pure-active-power operation are, respectively, 23.0% and 10.0% lower than that of MMC in inverter and rectifier modes. When the converter also compensates 0.5 p.u. inductive var to the ac grid, MDC has the loss-rate benefit of 11.2% over MMC in inverter mode and similar loss-rate with MMC in rectifier mode.

With a medium load, both the two converters realize their lowest loss rates. As the load grows heavier, the loss rates rise since the conduction losses of the devices quadratically increase with the current. When the load rate is lower than 20%, the constant power loss on static voltage-sharing resistors leads to high loss rates.

It is also noted that under the same transmission direction and load rate, the power loss of MDC increases with a decreased power factor, while that of MMC reduces. This is consistent with the current model in Fig. 2.

C. Reliability

Although the high number of SDMs in MDC rises the total quantity of submodules, the decrease of fully controlled device number compensates the disadvantage to some extent. Hence, MDC may not have a lower reliability than MMC. Assuming a same failure rate of fully controlled devices, gate drivers, floating supplies, and local controllers in the modules, MDC has a similar failure rate with MMC.

Modular-designed series connection is adopted in all the arms of MDC. Therefore, it is possible to realize a dynamic redundancy alike MMC. A certain proportion of redundant modules are retained and participate in the operation. The malfunctioned modules can be bypassed by closing a bypass switch or breaking down the IGCT [30] to ensure a reliable continuous operation of the converter.

In addition, cross-redundancy of floating supply and local controller between adjacent modules is hopeful to further improve the reliability of MDC, which is also a promising research direction.

D. Limitations and Further Applying Guidelines

The SDM aims to solve the problems of series connection and floating supply. From the converter point of view, an SDM can still be seen as a reverse-conducting device, which conducts bidirectionally but blocks unidirectionally. Therefore, it cannot bring any ability in dc-side fault blocking. It will be helpful for fault blocking to use bidirectional blocking arms, for example, to replace the main devices in the SDMs with two reverse-blocking IGCTs in inverse parallel. This will be valuable in overhead-line-based HVdc transmission [31], [32].

In HVdc, hundreds of devices in series are required. The ZVS characteristic in MDC and application of the proposed SDM solve the series-connection problem without the need of device selection. Nevertheless, it is still recommended to form each bridge arm with the devices of the same model and batch in order to facilitate the voltage sharing. Moreover, to choose devices with similar parameters in turn-OFF delay time, turn-OFF energy per pulse, and leakage current will be helpful to further reduce the configuration of passive devices in the SDMs [33].

TABLE IV
COMPARISON BETWEEN VSC TOPOLOGIES FOR HVDC

Item	PWM-VSC	MMC	MDC
Cost	★★★★★	★	★★★
Efficiency	★	★★★★	★★★★★
Volume	★★★★★	★	★★★
feasibility	★[&]	★★★★★	★★★★★

[&]The series connection of hundreds of devices with hard-switching PWM causes the technical bottleneck.

E. Comprehensive Comparison

Based on the analysis above, a comprehensive comparison between MDC and common VSC topologies for HVdc application is carried on. The results are shown in Table IV, which demonstrate a balanced technical advantage of MDC. Especially, MDC tends to be superior in most aspects than its competing topology MMC.

VIII. CONCLUSION

The proposed MDC has significant advantages in volume, as well as benefits in cost and efficiency. The SDM matches perfectly with the quasi-soft switching characteristics in MDC, for which it can maintain the energy balance during operation, without overvoltage or undervoltage. It realizes voltage sharing in the H-bridge of MDC, while providing floating supply for secondary circuits and device drivers. It solves a key problem of MDC toward engineering application. Finally, the implementation and experiment of the power MDC prototype verify the correctness of the theoretical analysis and the feasibility of the proposal.

The future research can focus on the electrical stress of MDC under various transient conditions and ensure the universality of the proposed scheme in VSC-HVdc.

APPENDIX

Calculation Method of Device Current in Submodules

The specific device through which the current flows in the half-bridge submodule is determined by the instantaneous current direction and switching state of the submodule, as is shown in Fig. 2(a). The switching state of each submodule cannot be accurately analyzed in theory under the nearest-level modulation.

However, the probability of each module to be switched IN and OUT at a specific moment can be characterized in the statistical sense by the instantaneous value of the modulation wave. For example, if the instantaneous value of the modulation wave of a cascaded-submodules is 0.72, then 72% of the total submodules ought to be switched in. In other words, the possibility of each submodule to be switched IN is 72%, while the possibility to be switched OUT is 28%.

In MMC, the modulation waveform of lower arm in phase A can be expressed as

$$k(t) = [1 + m\sin(\omega t + \varphi)]/2 \tag{4}$$

in which m, ω, and φ stand for the modulation ratio, the angular frequency, and the phase-shift angle, separately. Then at the moment t, it can be considered that the switched-IN probability of for each module is P_{IN}

$$P_{\mathrm{IN}}(t) = k(t) \tag{5}$$

and the switched-OUT probability is P_{OUT}

$$P_{\mathrm{OUT}}(t) = 1 - P_{\mathrm{IN}}(t). \tag{6}$$

If we denote the current of the submodule as i_{SM}, and define the signal function

$$S(x) = \begin{cases} 1, \text{if} x \geq 0 \\ 0, \text{if} x < 0. \end{cases} \tag{7}$$

The rms current of the four devices in the submodule can be calculated by the following equations:

$$I_{\mathrm{T1}} = \sqrt{\frac{1}{T}\int_T i_{\mathrm{SM}}^2(t)\, P_{\mathrm{IN}}(t)\{1 - S[i_{\mathrm{SM}}(t)]\}\,\mathrm{d}t} \tag{8}$$

$$I_{\mathrm{D1}} = \sqrt{\frac{1}{T}\int_T i_{\mathrm{SM}}^2(t)\, P_{\mathrm{IN}}(t)\, S[i_{\mathrm{SM}}(t)]\,\mathrm{d}t} \tag{9}$$

$$I_{\mathrm{T2}} = \sqrt{\frac{1}{T}\int_T i_{\mathrm{SM}}^2(t)\, P_{\mathrm{OUT}}(t)\, S[i_{\mathrm{SM}}(t)]\,\mathrm{d}t} \tag{10}$$

$$I_{\mathrm{D2}} = \sqrt{\frac{1}{T}\int_T i_{\mathrm{SM}}^2(t)\, P_{\mathrm{OUT}}(t)\{1 - S[i_{\mathrm{SM}}(t)]\}\,\mathrm{d}t}. \tag{11}$$

To obtain the current of devices in MDC, we only need to change the modulation waveform function according to its operation principle

$$k(t) = A[m\sin(\omega t + \varphi)] \tag{12}$$

in which $A(x)$ refers to the absolute-value function

$$A(x) = \begin{cases} x, \text{if } x \geq 0 \\ -x, \text{if } x < 0. \end{cases} \tag{13}$$

REFERENCES

[1] Y. Fu, Y. Liu, L. -l. Huang, F. Ying, and F. Li, "Collection system topology for deep-sea offshore wind farms considering wind characteristics," *IEEE Trans. Energy Convers.*, vol. 37, no. 1, pp. 631–642, Mar. 2022.

[2] M. Aragüés Peñalba, O. Gomis-Bellmunt, and M. Martins, "Coordinated control for an offshore wind power plant to provide fault ride through capability," *IEEE Trans. Sustain. Energy*, vol. 5, no. 4, pp. 1253–1261, Oct. 2014.

[3] H. Wu, J. Yu, J. Liu, R. Mei, X. Ji, and H. Wang, "Voltage control of offshore wind farm considering reactive ability of electrochemical energy storage," in *Proc. IEEE Sustain. Power Energy Conf.*, 2022, pp. 1–5.

[4] L. Wang and M. S. Nguyen Thi, "Comparative stability analysis of offshore wind and marine-current farms feeding into a power grid using HVDC links and HVAC line," *IEEE Trans. Power Del.*, vol. 28, no. 4, pp. 2162–2171, Oct. 2013.

[5] G.-L. Lu, C.-H. Lin, and Y.-K. Wu, "Comparison of communication-based and coordination-based frequency control schemes for HVdc-connected Offshore Wind Farms," *IEEE Trans. Ind. Appl.*, vol. 57, no. 4, pp. 3352–3365, Jul./Aug. 2021.

[6] F. An et al., "DC cascaded energy storage system based on DC collector with gradient descent method," *IEEE Trans. Ind. Electron.*, vol. 71, no. 2, pp. 1594–1605, Feb. 2024.
[7] S. Debnath, J. Qin, B. Bahrani, M. Saeedifard, and P. Barbosa, "Operation, control, and applications of the modular multilevel converter: A review," *IEEE Trans. Power Electron.*, vol. 30, no. 1, pp. 37–53, Jan. 2015.
[8] A. Beddard, M. Barnes, and R. Preece, "Comparison of detailed modeling techniques for MMC employed on VSC-HVDC schemes," *IEEE Trans. Power Del.*, vol. 30, no. 2, pp. 579–589, Apr. 2015.
[9] F. Z. Peng and J.-S. Lai, "Dynamic performance and control of a static VAr generator using cascade multilevel inverters," *IEEE Trans. Ind. Appl.*, vol. 33, no. 3, pp. 748–755, May/Jun. 1997.
[10] Y. Tang, M. Chen, and L. Ran, "A compact MMC submodule structure with reduced capacitor size using the stacked switched capacitor architecture," *IEEE Trans. Power Electron.*, vol. 31, no. 10, pp. 6920–6936, Oct. 2016.
[11] G.-J. Su, "Multilevel DC-link inverter," *IEEE Trans. Ind. Appl.*, vol. 41, no. 3, pp. 848–854, May/Jun. 2005.
[12] J. A. Ferreira, "The Multilevel modular DC converter," *IEEE Trans. Power Electron.*, vol. 28, no. 10, pp. 4460–4465, Oct. 2013.
[13] B. Zhao, Q. Song, J. Li, and W. Liu, "A modular multilevel DC-link front-to-front DC solid-State transformer based on high-frequency dual active phase shift for HVDC grid integration," *IEEE Trans. Ind. Electron.*, vol. 64, no. 11, pp. 8919–8927, Nov. 2017.
[14] B. Zhao et al., "A multilevel DC-link converter for VSC-HVDC application," in *Proc. 25th Eur. Conf. Power Electron. Appl.*, 2023, pp. 1–10.
[15] T. Wang, H. Lin, S. Liu, and M. Zhao, "An active voltage balance method based on adjusting driving signals time delay for series-connected IGBTs," *IEEE J. Emerg. Sel. Topics Power Electron.*, vol. 9, no. 6, pp. 6748–6760, Dec. 2021.
[16] V. U. Pawaskar, G. Gohil, and P. T. Balsara, "Study of voltage balancing techniques for series-connected insulated gate power devices," *IEEE J. Emerg. Sel. Topics Power Electron.*, vol. 10, no. 2, pp. 2380–2394, Apr. 2022.
[17] G. Belverde, A. Galluzzo, M. Melito, S. Musumeci, and A. Raciti, "Snubberless voltage sharing of series-connected insulated-gate devices by a novel gate control strategy," *IEEE Trans. Power Electron.*, vol. 16, no. 1, pp. 132–141, Jan. 2001.
[18] V. Jones, R. A. Fantino, and J. C. Balda, "A modular switching position with voltage-balancing and self-powering for series device connection," *IEEE J. Emerg. Sel. Topics Power Electron.*, vol. 9, no. 3, pp. 3501–3516, Jun. 2021.
[19] Z. Gao, S. Shao, W. Cui, J. Zhang, X. Chen, and K. Sheng, "A voltage balancing method for series-connected power devices based on active clamping in voltage source converters," *IEEE Trans. Power Electron.*, vol. 37, no. 9, pp. 10620–10632, Sep. 2022.
[20] J.-F. Chen, J.-N. Lin, and T.-H. Ai, "The techniques of the serial and paralleled IGBTs," in *Proc. IEEE IECON. 22nd Int. Conf. Ind. Electron., Control, Instrum.*, 1996, vol. 2, pp. 999–1004.
[21] S. Bhattacharya, "Comparative evaluation of IGCT and GTO thyristor for series connection in high power voltage source inverter based FACTS applications," in *Proc. Eur. Conf. Power Electron. Appl.*, 2007, pp. 1–9.
[22] T. Wei, Q. Song, J. Li, B. Zhao, Z. Chen, and R. Zeng, "Experimental evaluation of IGCT converters with reduced di/dt limiting inductance," in *Proc. IEEE Appl. Power Electron. Conf. Expo.*, 2018, pp. 1710–1716.
[23] R. Zeng et al., "Integrated gate commutated thyristor-based modular multilevel converters: A promising solution for high-voltage dc applications," *IEEE Ind. Electron. Mag.*, vol. 13, no. 2, pp. 4–16, Jun. 2019.
[24] "ST2000GXH31," Toshiba, Singapore, 2020. [Online]. Available: https://toshiba.semicon-storage.com/ap-en/semiconductor/product/igbts-iegts/iegt-ppi/detail.ST2000GXH31.html
[25] "5SHX-36l4521," 2020. [Online]. Available: https://publisher.hitachienergy.com/preview?DocumentID=5SYA1256&LanguageCode=en&DocumentPartId=&Action=Launch
[26] "Failure rates of IGCTs due to cosmic rays, application Note 5SYA 2046-03," Hitachi Energy, Zürich, Switzerland, 2019. [Online]. Available: https://publisher.hitachienergy.com/preview?DocumentID=5SYA2046&LanguageCode=en&DocumentPartId=&Action=launch&DocumentRevisionId=C
[27] L. Yang et al., "A simplified analytical calculation model of average power loss for modular multilevel converter," *IEEE Trans. Ind. Electron.*, vol. 66, no. 3, pp. 2313–2322, Mar. 2019.
[28] B. Zhao et al., "Practical analytical model and comprehensive comparison of power loss performance for various MMCs based on IGCT in HVDC application," *IEEE J. Emerg. Sel. Topics Power Electron.*, vol. 7, no. 2, pp. 1071–1083, Jun. 2019.
[29] J. Qin and M. Saeedifard, "Reduced switching-frequency voltage-balancing strategies for modular multilevel HVDC converters," *IEEE Trans. Power Del.*, vol. 28, no. 4, pp. 2403–2410, Oct. 2013.
[30] J. Liu et al., "A novel controlled punch-through IGCT for modular multilevel converter with overvoltage bypass function," *IEEE Trans. Power Electron.*, vol. 36, no. 7, pp. 8280–8290, Jul. 2021.
[31] Y. Xue and Z. Xu, "On the bipolar MMC-HVDC topology suitable for bulk power overhead line transmission: Configuration, control, and DC fault analysis," *IEEE Trans. Power Del.*, vol. 29, no. 6, pp. 2420–2429, Dec. 2014.
[32] S. Cui and S.-K. Sul, "A comprehensive DC short-circuit fault ride through strategy of hybrid modular multilevel converters (MMCs) for overhead line transmission," *IEEE Trans. Power Electron.*, vol. 31, no. 11, pp. 7780–7796, Nov. 2016.
[33] "Applying IGCTs, Application Note 5SYA 2032-04," Hitachi Energy, Zürich, Switzerland, 2016. [Online]. Available: https://publisher.hitachienergy.com/preview?DocumentID=5SYA2032&LanguageCode=en&DocumentPartId=&Action=launch&DocumentRevisionId=D

Ruihang Bai (Graduate Student Member, IEEE) was born in Xi'an, China, in 1998. He received the B.S. degree in electrical engineering, in 2020, from Tsinghua University, Beijing, China, where he is currently working toward the Ph.D. degree in electrical engineering.

His research interests include high power converter, high power semiconductor device, and VSC-HVdc system.

Biao Zhao (Senior Member, IEEE) was born in Hubei, China, in 1987. He received the B.S. degree from the Dalian University of Technology, Dalian, China, in 2009, and the Ph.D. degree from the Tsinghua University, Beijing, China, in 2014, both in electrical engineering.

He is currently an Associate Professor with the Department of Electrical Engineering, Tsinghua University, Beijing, China. His research interests include high power converter, high power semiconductor device, and flexible dc transmission and distribution system.

Xueyin Zhang was born in Sichuan, China, in 1992. He received the B.S. and Ph.D. degrees in electrical engineering from the Department of Electrical and Electronic Engineering, North China Electric Power University, Beijing, China, in 2015 and 2020, respectively.

He was a Visiting Scholar with FREEDM System Center, North Carolina University, Chapel Hill, NC, USA, from 2018 to 2019.He is currently a power electronic converter R&D Engineer of Tsinghua Sichuan Energy Internet Research Institute, Tsinghua University, Beijing, China. His research interests include high power converter, high power semiconductor device, and flexible dc transmission and distribution system.

Lu Qu (Member, IEEE) was born in 1987. He received the Ph.D. degree in electrical engineering from the University of Chinese Academy of Sciences, Hefei, China, in 2016.

He is currently an Associate Researcher with Tsinghua University, Beijing, China. His research interests include dc grid and dc breaking technology

Jinpeng Wu was born in Hebei, China, in 1987. He received the B.S. and Ph.D. degrees in electrical engineering from the Department of Electrical Engineering, Tsinghua University, Beijing, China, in 2010 and 2015, respectively.

From 2016 to 2020, he continued his research with Stanford University, Stanford, CA, USA, and Lawrence Berkeley National Lab, Berkeley, CA, USA, as a Postdoctoral Researcher. He is currently an Assistant Professor with the Department of Electrical Engineering, Tsinghua University. His research interests include the energy and electrical materials, power electronics, and X-ray spectroscopies.

Zhanqing Yu (Member, IEEE) was born in Inner Mongolia, China, in 1981. He received the B.Sc. and Ph.D. degrees in electrical engineering from Tsinghua University, Beijing, China, in 2003 and 2008, respectively.

In 2008, he became a Post doctor with the Department of Electrical Engineering, Tsinghua University, Beijing, China, where he became a Lecturer, in 2010, and an Associate Professor, in 2012. His research interests include dc grid, dc breaker, electromagnetic environment and electromagnetic compatibility, and lightning protection.

Qiang Song (Senior Member, IEEE) was born in Changchun, China, in 1975. He received the B.E.E. and Ph.D. degrees in electrical engineering from the Tsinghua University, Beijing, China, in 1998 and 2003, respectively.

From 2003 to 2008, he was a Lecturer with the Department of Electrical Engineering, Tsinghua University. Since 2008, he has been an Associate Professor with the Department of Electrical Engineering, Tsinghua University. His research interests include high-power electronic interfaces for utility system, flexible ac transmission system, VSC-HVdc system, and custom power quality.

Rong Zeng (Senior Member, IEEE) was born in Shaanxi, China, in 1971. He received the B.Eng., M.Eng., and Ph.D. degrees from the Department of Electrical Engineering, Tsinghua University, Beijing, China, in 1995, 1997, and 1999, respectively, all in electrical engineering.

In 1999, he was a Lecturer with the Department of Electrical Engineering, Tsinghua University, where he became an Associate Professor, in 2002, and a Professor, in 2007. His research interests include airgap discharge, lightning protection, and electromagnetic compatibility in power systems, electric and magnetic field measurement by integrated electro-optical sensors, power semiconductor, HVdc system, and direct current circuit breaker.